J. Fluid Mech. (2008), *vol.* 615, *pp.* 101–120.
doi:10.1017/S0022112008003765 Printed in the United Kingdom

Turbulent flow similarity over an array of cubes in near-neutrally stratified atmospheric flow

A. INAGAKI AND M. KANDA

Department of International Development Engineering, Tokyo Institute of Technology, Tokyo, Japan
inagaki.a.ab@m.titech.ac.jp

(Received 16 August 2007 and in revised form 28 July 2008)

The main objective of this study is to examine the robustness of the inner-layer scaling similarity of near-wall turbulence. The turbulent boundary layer of interest is over a very rough surface with a very high Reynolds number and significant outer-layer disturbances. This is not consistent with the canonical turbulent flows studied in laboratories, but it is common in urban areas. The investigation was conducted using the comprehensive outdoor scale model (COSMO) facility. COSMO is composed of a regular array of 1.5 m concrete cubes on a $50 \times 100\,\mathrm{m}^2$ flat concrete base. This unique facility allows us to obtain the turbulent dataset within the vertical constant stress region under near-neutral stratification at high Reynolds numbers. The turbulent spectra and the standard deviation of velocity fluctuations from COSMO were compared with the values obtained over rural and urban surfaces, and in wind-tunnel experiments.

The results confirmed that the inner-layer scaling similarity was robust for the wall-normal fluctuations and the Reynolds stress, independent of the roughness types and the outer-layer conditions. The inner-layer scaling similarity failed for the horizontal velocity fluctuations owing to the influence of the outer-layer disturbance. The relative importance of outer-layer turbulence to inner-layer-scale eddies in the horizontal velocity fluctuations was successfully quantified in terms of the roughness scale normalized by the outer-layer scale.

1. Introduction

This paper investigates turbulent flow similarity over rough walls, with a special focus on flows over cubical obstacles. Understanding turbulent flows over rough walls is important in industrial applications involving flows in channels and pipes, and in atmospheric studies dealing with geophysical surfaces that are usually rough. The characteristics of rough-wall turbulent boundary layers have been thoroughly studied in wind-tunnel experiments (reviewed by Raupach, Antonia & Rajagopalan 1991; Jimenez 2004), field observations (reviewed by Finnigan 2000 for vegetation; Roth 2000 for cities) and numerical simulations (e.g. direct numerical simulations by Miyake, Tsujimoto & Nakaji 2001; Nagano, Hattori & Houra 2004; Krogstad *et al.* 2005; Coceal *et al.* 2006; large-eddy simulations by Hanna *et al.* 2002; Cui, Patel & Lin 2003; Kanda, Moriwaki & Kasamatsu 2004; Kanda 2006). These studies considered different types of flow, including flows in channels, in ducts, in pipes and over geophysical surfaces, and used different Reynolds numbers, flow boundary conditions above the boundary layer (e.g. free surface, free stream, flows of various

turbulence intensities and convection above the boundary layer) and different types of surface roughness. A composite of various data sources would be useful for examining the validity of fundamental similarity theories. Our study differs from the conventional set-ups mentioned above in that we deal with a unique dataset of turbulent flows over building-like roughness derived from an outdoor reduced urban scale model experiment to give new insights into the scale similarity of rough-wall turbulent flows, specifically considering the influence of large roughness, large Reynolds number and strong outer-layer disturbances.

This study investigated the turbulence similarity in the inertial sublayer scaled on the inner-layer variables. This is like Townsend's wall similarity (e.g. Raupach *et al.* 1991) or the Monin–Obukhov similarity (e.g. Kaimal *et al.* 1972) under neutral stratification and using high-Reynolds-number turbulent flow. The inner-layer scale is the scale that determines the characteristics of eddies originating at the wall surface. Under neutral stratification, the surface friction velocity, u_* and the wall-normal height from the ground surface, z, are generally specified by their velocity scales and length scales, respectively. The outer scale is the scale for turbulence in the outer-layer above the turbulent boundary layer, and the outer length scale is specified by the whole flow region such as the boundary-layer thickness δ. The friction velocity and free-stream velocity have been studied as possible velocity scales of outer-layer turbulence, but this scale is still not completely understood (e.g. Akinlade *et al.* 2004). Furthermore, the origin of the outer-layer turbulence is not yet clear for a canonical turbulent boundary layer.

The inner-layer scale similarity provides universal functions or constants for turbulent statistics. Townsend (1976) proposed two theoretical hypotheses to support inner-layer scale similarity for neutrally stratified flow. These are the 'wall turbulence similarity' and 'equilibrium layer'. The wall-turbulence similarity hypothesis proposes that the turbulent motions above the roughness sublayer at a high Reynolds number, in which the roughness has a direct dynamic influence, are independent of the roughness except for the inner- and outer-layer scaling parameters. Laboratory experiments have confirmed this hypothesis (Perry & Abell 1977; Raupach *et al.* 1991). Within the equilibrium layer, the rates of turbulent kinetic energy (TKE) production and dissipation are exceptionally large compared with those in other parts of the flow, and almost balance. At that point, the boundary-layer thickness as an outer-layer scale becomes irrelevant to the turbulent motions involved with the energy production and dissipation (Townsend 1961). Raupach *et al.* (1991) used wind-tunnel and atmospheric experiments to confirm the universal constant for the inner-scaled standard deviations of velocity components in the equilibrium layer over various types of roughness. Another perspective of the inner-layer scaling similarity was provided by Bradshaw (1967*a*, *b*). He investigated this similarity in an equilibrium layer over a range of pressure gradients by dividing the inner-layer turbulence into two types. The active components follow the inner-layer scaling variables and are responsible for the vertical turbulence transfer. The inactive components come from the effect of the outer-layer disturbance. The inactive eddies contributed to horizontal velocity fluctuations, but not to vertical velocity fluctuations or momentum transfer.

Inner-layer scale similarity has also been investigated in the constant stress layer of the atmospheric boundary layer (ABL). The ABL can be roughly divided into two layers (Stull 1988). The upper layer is the mixed layer where the turbulence is usually convectively driven and is bounded on its upper surface by the free atmosphere. The atmospheric surface layer (ASL) is on the bottom of the mixed layer where the turbulence under neutral stratification is mechanically shear driven. The

geographical surface is usually rough so that the ASL can be further subdivided into two more layers: the roughness sublayer adjacent to the roughness (Raupach, Thom & Edwards 1980) and the inertial or logarithmic layer above the roughness sublayer. In the roughness sublayer, the flow is dynamically influenced by roughness, and the mean flow field has a three-dimensional variation. The flow within the inertial layer is horizontally homogeneous and has a vertical logarithmic variation of mean velocity with constant Reynolds stress.

The inner-layer scaling similarity is useful for expressing turbulent motions in the constant stress layer, which is a type of equilibrium layer (Townsend 1961). Monin–Obukhov similarity (MOS) is based on the inner-layer scaling and is often used in meteorological studies because of its ability to explain the effect of thermal stratification. MOS has been tested in horizontally homogeneous and flat fields (Kaimal *et al.* 1972); these studies demonstrated that the Reynolds stress and the wall-normal velocity fluctuation normalized with inner-layer scaling reduce to the same curves except for horizontal velocity fluctuations. The horizontal velocity fluctuations are affected only by the outer inactive turbulence (Panofsky *et al.* 1978). MOS has also been applied to turbulent statistics over urban regions (Högström, Bergström & Alexandersson 1982; Rotach 1993; Roth & Oke 1993; Roth 1993). The geometric surface conditions in urban areas can be represented by an array of massive roughness that is horizontally heterogeneous. Nevertheless, the results obtained using inner-layer scaling showed similarities to those obtained for flat homogeneous fields where they were above the roughness sublayer (Roth 2000).

The purpose of this study is to give new insights into the inner-layer scaling law over a fully rough surface using a comprehensive outdoor scale model (COSMO) experiment for an urban environment. COSMO can provide a unique dataset obtained under atmospheric conditions with an intermediate scale of roughness, thereby filling the gap between indoor and field experiments.

For fluid mechanics, the surface condition used in this study is classified as extremely rough and the Reynolds number is very high; the roughness Reynolds number $Re^*(=z'u_*/\nu)$ is usually about 10^4–10^5. The flow structure above the inertial sublayer differs considerably between indoor and outdoor conditions. The former is normally free-stream or bounded by a rigid lid, while the latter is usually bounded by a convective layer. The question remains as to whether the mixed layer turbulence is really inactive as predicted by Bradshaw (1967*b*), an issue addressed by this study.

From a meteorological perspective, COSMO is essentially a simplified city. The regular array of cubes is free of many real-life uncertainties such as the irregular arrangement of buildings, complex land use and the effect of human activities. The obstacle scale, which is $1/5$ of the typical residential building height in Japan, is expected to be successful in decoupling the inner- and outer-layer scale turbulences. In the ABL, the vertically constant stress layer can develop up to a height of $0.1z_i$, where z_i is the mixed-layer depth whose height is about 100–1000 m. If the obstacle height is close to $0.1z_i$, the roughness sublayer penetrates the bottom of the mixed layer and the constant stress region may not exist (Rotach 1999). Such a situation is likely to occur in real cities where the building height is of the order of tens of metres and the roughness sublayer develops several times higher than the building height. Thus, the validity of the inner-layer scaling similarity over cities can be re-examined under controlled conditions with $1/5$ scale models.

Using the unique COSMO dataset with field and indoor datasets, we examined the inner-layer scaling similarity over a fully rough surface including the effects of roughness and outer-layer turbulence.

2. Theoretical background

We define streamwise, spanwise and wall-normal coordinates in the form (x, y, z). The mean wind velocity vectors and fluctuating velocity vectors are (U, V, W) and (u, v, w), respectively. Similarly, Θ and θ are the mean absolute and fluctuating components of temperature.

2.1. *Monin–Obukhov similarity theory*

We evaluated the turbulent characteristics based on the MOS framework. Within the inertial sublayer over a horizontally homogeneous surface, any turbulent statistics are represented by a function of the inner-layer variables, which are the height z (m), the friction velocity u_* (m s^{-1}), the buoyancy parameter g/Θ (k^{-1} m s^{-2}) and the surface heat flux $\overline{w\theta}$ (k m s^{-1}). The overbar denotes the temporal average and g is the acceleration due to gravity (m s^{-2}). The combination of these variables provides a non-dimensional parameter ξ defined as

$$\xi = \frac{z'}{L} = -\frac{(g/\Theta)(\overline{w\theta})}{u_*^3/kz'}, \tag{1}$$

where L is the Obukhov length (m) and z' is the effective height (m) defined as the difference between the actual height z and the displacement height d (m), which is the effective origin of z owing to the flow displacement over the roughness elements. Theoretically, it is defined as the mean height of the momentum absorbed by the surface (Thom 1971). The parameter k is the von Kármán constant; we used a value of 0.4 in this study.

The value ξ represents the stability of the thermal stratification. In the MOS framework, turbulent statistics are expressed as a function of the single parameter ξ. Therefore, any turbulent statistics with inner-layer scaling become constant-independent under neutral stratification (i.e. $\xi = 0$).

This relationship is also derived from a combination of the wall-turbulence similarity and the equilibrium-layer hypothesis for high-Reynolds-number turbulent motion (Townsend 1961, 1976). The Reynolds number is usually very high in the atmosphere.

2.2. *Turbulent spectra*

Based on MOS, Kaimal *et al.* (1972) provided empirical formulae for the turbulent spectra and cospectra based on their rural experiments over flat and horizontally homogeneous terrain. These formulae with neutral condition pre-multipliers are

$$fS_u(f)/u_*^2 = 105f'(1+33f')^{-5/3}, \tag{2}$$

$$fS_v(f)/u_*^2 = 17f'(1+9.5f')^{-5/3}, \tag{3}$$

$$fS_w(f)/u_*^2 = 2f'(1+5.3f'^{5/3})^{-1}, \tag{4}$$

$$-fCo_{uw}(f)/u_*^2 = 12f'(1+9.6f')^{-7/3}, \tag{5}$$

where f is the natural frequency (s^{-1}); S_u, S_v and S_w are the streamwise, spanwise and wall-normal spectral densities; and Co_{uw} is the cospectral density of the Reynolds stress (m^2 s^{-2}). The parameter f' is an inner-scaled non-dimensional frequency, i.e. $f' = fz'/U$ assuming the frozen turbulence hypothesis.

2.3. *Standard deviation of the turbulent fluctuations*

The standard deviations of the velocity fluctuations, $\sigma_u = (\overline{u^2})^{1/2}$, $\sigma_v = (\overline{v^2})^{1/2}$, or $\sigma_w = (\overline{w^2})^{1/2}$ normalized by the friction velocity, reduce to constants under neutral

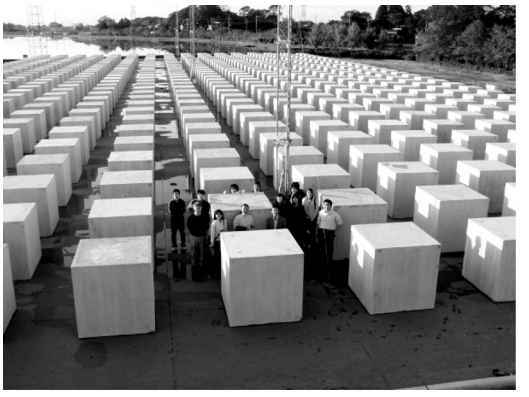

FIGURE 1. Photograph of the COSMO site taken from the northwest side. The cubes are 1.5 m high.

stratification according to the MOS framework. However, some field experiments have indicated that it does not become constant for the horizontal velocity components even under neutral stratification, owing to the propagation of the prominent outer-layer disturbance, which is the convective motion in the ABL (Kaimal *et al.* 1972). Clarke, Ching & Godowitch (1982) proposed an empirical formula for the streamwise velocity fluctuation under neutral stratification,

$$\sigma_u/u_* = C_u \left(\frac{\lambda_{max,u}}{kz'} \right)^{1/3}, \tag{6}$$

where $\lambda_{max,u}$ is the peak wavelength of the streamwise velocity spectra and C_u is a constant. Clarke *et al.* assumed that $\lambda_{max,u}$ is a function of the ABL depth and represents the strength of the outer-layer disturbance.

3. Experimental set-up

3.1. *COSMO*

The COSMO experimental facility was constructed at the Nippon Institute of Technology in Saitama, Japan. Figure 1 is a photograph of the experimental site. The upwind side is open to a harvested rice field that extends out about 500 m from the edge of COSMO. The model is composed of a flat rectangular foundation plate with 512 cubes on it. The plate and blocks are all made of concrete. The plate is 50 m $\times$ 100 m. The cubes sides are 1.5 m ($= H$), which is about 1/5 the scale of typical residential buildings in Japan. The cubes are arranged regularly to give a ratio of plan area of cubes to lot area of 0.25. Three 8 m meteorological towers are centrally lined up along the NW–SE axis. A schematic of the site is shown in figure 2.

3.2. *Data acquisition*

To measure the turbulent fluctuations in COSMO, we used five Kaijo sonic anemometer-thermometers (KAIJO DA-600 and TR90AH probe). The instruments were custom-ordered for this experiment with pass lengths between the transducers of 5 cm and sampling rates of 50 Hz. The variations among the instruments were measured onsite and are summarized in table 1. During this test, 5 sonic anemometers were installed 1 m above the flat plate and sampled at 50 Hz for two weeks. The table includes the ensemble averages of the 47 30-min sets of integrated statistics.

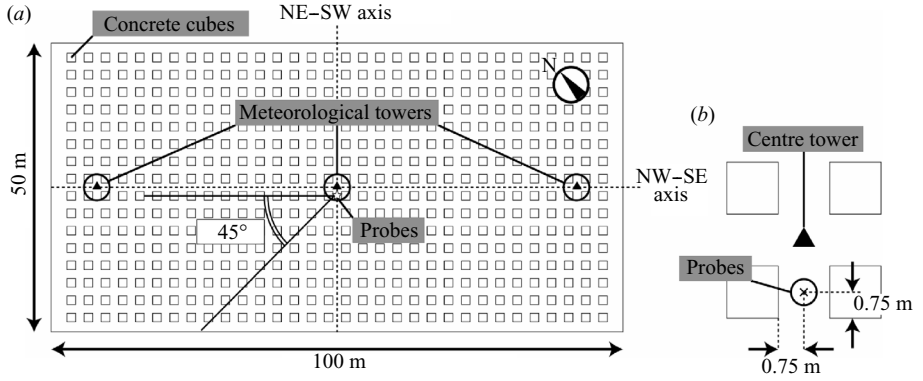

FIGURE 2. Schematic of the COSMO site. The roughness cubes are aligned regularly for a building area density of 0.25. Meteorological towers are installed at three locations, and probes for the sonic anemometers are installed on the centre tower. An angle of 45° to the probes indicates an acceptable mean wind direction for the analysis. (*b*) The relative location of the probes and cubes.

Symbol	Standard deviation
U (m s^{-1})	0.050
σ_u (m s^{-1})	0.011
σ_v (m s^{-1})	0.007
σ_w (m s^{-1})	0.005
u_* (m s^{-1})	0.011

TABLE 1. Statistical differences of the 5 Kaijo-DA600 sonic anemometers.

The sampling frequency was not sufficient to resolve up to the viscous dissipation range and it caused an underestimation of σ_u, σ_v and σ_w. However, the errors in these integrated variables were less than few per cent of the total magnitude, which was estimated by extrapolating the $-2/3$ spectral curve asymptotically to the horizontal axis and then integrating the area between the extrapolation curve and the horizontal axis with a log–linear plot, making them almost irrelevant to the results of our study.

The sonic anemometers were installed on the centre tower in a vertical line at heights of 6.0, 4.5, 3.0, 2.25 and 1.5 m above the plate foundation. The ratios of anemometer height to the obstacle height were $4H, 3H, 2H, 1.5H$ and H, respectively. The horizontal location of the instruments was between two cubes, as shown in figure 2. The probe heads were directed parallel to the NW–SE street axis. Therefore, the fetch was about 50 m when the flow came from the northwest.

We took continuous measurements using this set-up between 16 December 2004 and 29 January 2005. During this time, the mean wind speed changed from 0 to 7.0 m s^{-1} and was usually directed from the northwest. The diurnal variation of the mean temperature was usually between 273 and 283 K on fair-weather days. The weather conditions were variable, ranging from fine to cloudy or rainy. The temporal mean statistics, and turbulent spectra and cospectra were calculated every 30 min during this period.

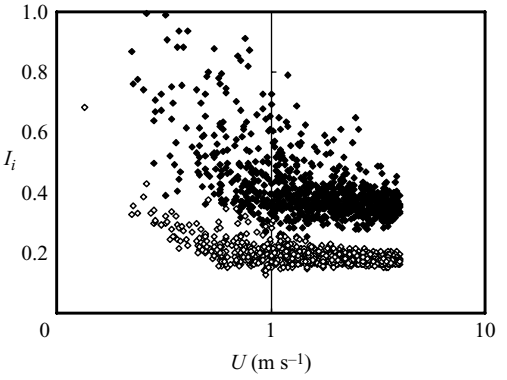

FIGURE 3. Turbulence intensities at $2H$ plotted on the horizontal mean velocity. Filled and open symbols are the streamwise velocity (I_u) and the wall-normal velocity (I_w) components, respectively.

3.3. *Data qualification*

Atmospheric flow has many fluctuations compared to the flow in a wind tunnel. This is typical of atmospheric turbulence. Since our aim was to examine the rough-wall boundary layer without significant advection, thermal, other body forcing, or experimental errors, the following data-screening criteria were adopted.

We trimmed our dataset using various criteria and thresholds. First, we completely excluded data obtained during periods of rain. We only kept data for a mean wind speed in the range 1–3 m s^{-1} at $2H$. This lower limit was due to the requirement of the frozen hypothesis to calculate the spectral wavelength when the turbulence intensity $I_u = \sigma_u/U$ was less than 0.5 (Willis & Deardorff 1976), and also served to eliminate exceptionally low Reynolds numbers. Figure 3 shows I_u and I_w plotted as functions of U for $2H$. The value of I_u was mostly less than 0.5, and the values of I_u and I_w (and also I_v, not shown) were almost independent of U when U was greater than 1 m s^{-1}. The upper limit of U was due to the limitation of the sampling frequency required to resolve the inertial subrange of the spectra, confirmed from the appearance of the $-5/3$ power law in the spectra. Flows from the NW–SE street axis and from an angle of 45° to that axis in the southwest direction (figure 2) were used for the analysis because flows from the northeast were affected by the arm of the platform. Additionally, the departure from the incident line of the probe head had to be less than 45° because of the configuration of the probe head. We also excluded data that had large variances during the averaging period to satisfy the analysis conditions for steady flow. The non-dimensional form of the inertia term of the TKE, $(kz'/u_*^3)\mathrm{d}\overline{e}/\mathrm{d}t$, should be less than 0.05 where $\overline{e} = 0.5(\overline{uu} + \overline{vv} + \overline{ww})$. This value is expected to be much smaller than the shear production term, which is usually 1.0 within the inertial layer under neutral stratification (Kaimal & Finnigan 1994). The turbulence intensity was almost independent of this parameter within the range of the threshold.

Our study focused on flow under neutral stratification. We restricted our analysis to times when the stability parameter was in the range of $-0.05 < \xi < 0.05$ at $2H$. We used this stability range to avoid the apparent stability dependence of the turbulent statistics. Also, we wished to compare our results with the urban reference of Roth (2000), which used the same definition.

After applying these restrictions, we were left with 48 30-min samples of mean statistics, which we ensemble averaged.

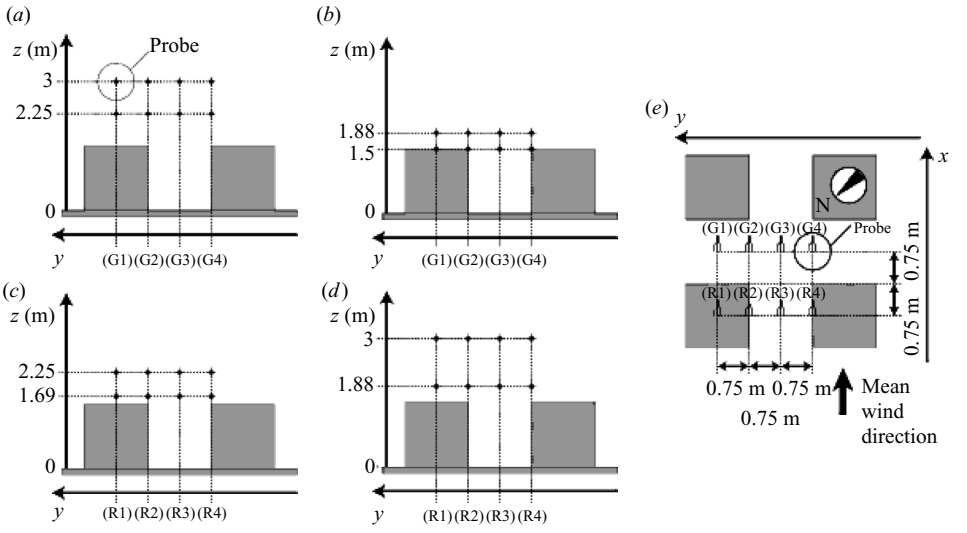

FIGURE 4. Schematic plan view of instrument layout for the preliminary experiment. (*a*)–(*d*) show the horizontal locations relative to the cubes, and (*e*) shows the horizontal location. (*a*)–(*d*) are different experimental periods. The locations G1, G2, G3 and G4 were aligned above the NW–SE street, where the measurements were conducted at $2\,H$, $1.5\,H$, $1.25\,H$ and H above the ground. The locations S1, S2, S3 and S4 were aligned above the cubes, where measurements were taken at $2\,H$, $1.5\,H$, $1.25\,H$ and $1.125\,H$ above the ground.

3.4. *Mean flow statistics*

Our first step was to estimate the roughness sublayer height. The concept of the roughness sublayer was introduced by Raupach *et al.* (1980, 1991) as the entire layer dynamically influenced by length scales associated with roughness elements. However, there is still no universally accepted definition of it in a practical sense. This study followed the definition by Cheng & Castro (2002) as the height where the horizontal heterogeneity of the turbulent statistics converges. Thus, the multipoint measurements were conducted at different relative locations in the same horizontal plane from the top of the obstacle to a height of $2\,H$.

The configuration of the instruments is shown in figure 4. Figure 4(*e*) shows the horizontal location of instruments, and figures 4(*a*)–4(*d*) indicate their vertical locations relative to the cubes. In this experiment, eight sonic anemometers were available simultaneously so that the measurements were made separately, as shown in figures 4(*a*)–4(*d*). The measurements were taken over different durations and compared to the main vertical distribution experiment. Points G1, G2, G3 and G4 were located above the NW–SE street and the measurement heights were $2\,H$, $1.5\,H$, $1.25\,H$ and H above the ground. Points R1, R2, R3 and R4 were above the centreline of the cubes aligned with the NW–SE street, and the measurement heights were $2\,H$, $1.5\,H$, $1.25\,H$ and $1.125\,H$ above the ground. The mean velocity and the standard deviations of the streamwise and vertical velocity fluctuations were normalized by the Reynolds stresses obtained at each location because there was no fixed measurement point for this experiment. However, the locally scaled variables at the same height should also reduce to a constant within the inertial layer. Figure 5 shows the vertical profiles of these non-dimensional variables. The variables above the roof (R1) were always the most diverse compared to those obtained at the other horizontal locations. The horizontal variations of each variable decrease dramatically moving upward from

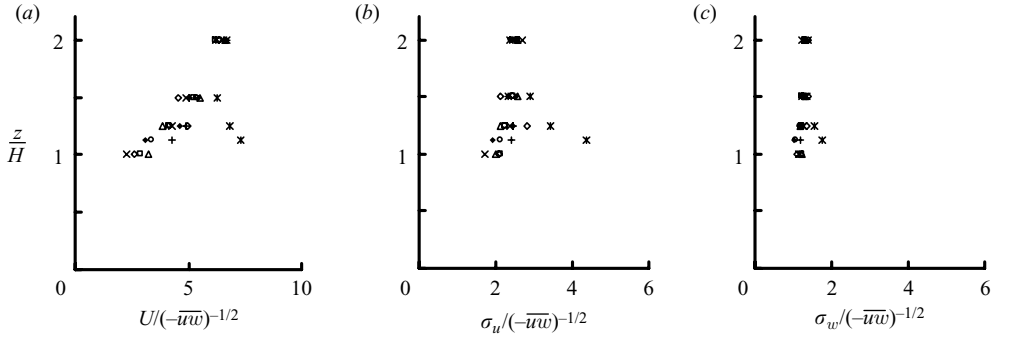

FIGURE 5. (*a*) Spatial variation of the mean velocity, (*b*) standard deviation of the streamwise velocity fluctuation, and (*c*) standard deviation of the vertical velocity fluctuation normalized by the square root of the Reynolds shear stresses. The symbols express the difference of the measurement locations corresponding to figure 4: ◇, G1; □, G2; △, G3; ×, G4; ∗, R1; ○, R2; +, R3; ◆, R4.

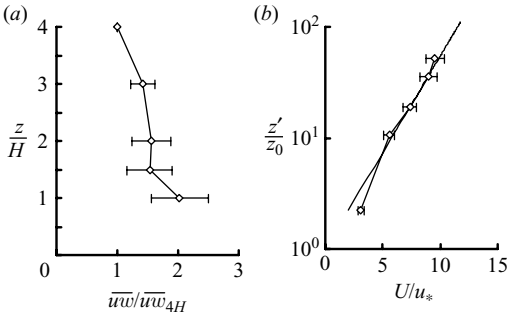

FIGURE 6. Vertical distributions of (*a*) the momentum flux and (*b*) the mean velocity. Momentum fluxes are normalized by the value obtained at $4\,H$, and mean velocities are normalized by the friction velocity. The diamonds with dashed lines are the values in COSMO and the solid line in (*b*) is the curve fitted to the values at $2\,H$ and $3\,H$, which are assumed to have a logarithmic variation.

the top of obstacles and almost converge to unity at a height of $2\,H$. Therefore, $2\,H$ is considered to be above the roughness sublayer for COSMO and $1.5\,H$ is somewhat in the roughness sublayer. This is consistent with wind-tunnel experiments using a similar roughness configuration (Cheng & Castro 2002). Although the vertical velocity fluctuation (figure 5*c*) at $1.5\,H$ appears almost to have converged, the value at R1 has a slight, but still the second largest, deviation from the others and it is difficult to judge the existence of the roughness sublayer using this variable.

Figures 6(*a*) and 6(*b*) show the vertical variation of $-\overline{uw}$ normalized by the value obtained at $4\,H$ and U/u_*, respectively. The value $-\overline{uw}$ is generally constant between $1.5\,H$ and $3\,H$ where the constant-stress layer is expected. Thus we estimated the friction velocity relevant to the inertial layer using the Reynolds stress at $2\,H$ as $u_* = (-\overline{uw})^{-1/2}$. The relatively larger value at H is because the value is not the horizontal average (e.g. Raupach, Coppin & Legg 1986), but is obtained at a single location behind the cube face where the shear stress is relatively strong compared to the other locations (figure 5*a*).

Considering the horizontal variation of turbulent statistics (figure 5) and the vertical distribution of momentum flux (figure 6*a*), the inertial sublayer in COSMO is expected

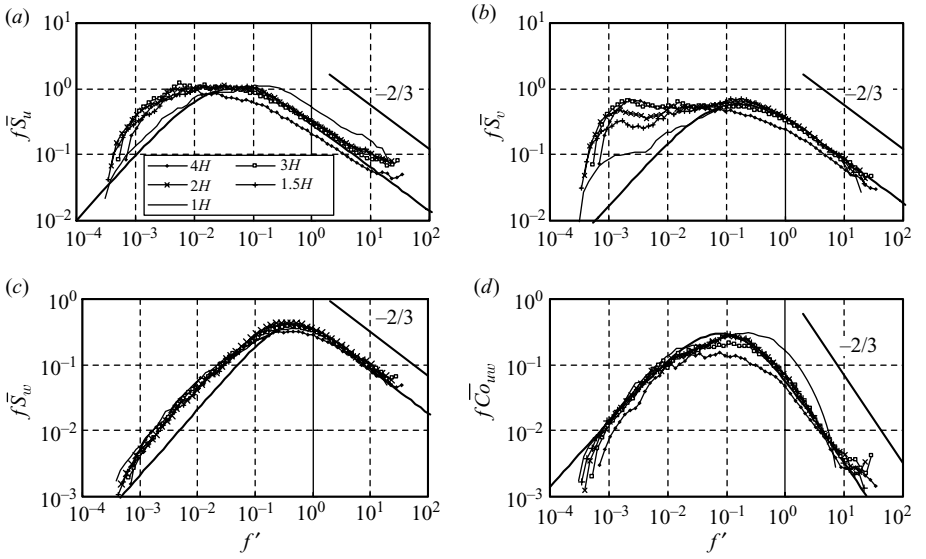

FIGURE 7. Pre-multiplied spectra and cospectra with inner-layer flow scaling obtained at each height in COSMO, plotted on log–log axes: (*a*) streamwise velocity spectra, (*b*) spanwise velocity spectra, (*c*) wall-normal velocity spectra, (*d*) cospectra of the Reynolds shear stress. The bold line represents the values obtained over a flat rural surface (Kaimal *et al.* 1972).

to be about $2\,H$ where the turbulent statistics are horizontally homogeneous and the momentum flux is vertically constant, which is expected to extend up to about $3\,H$.

Figure 6(*b*) shows the vertical variation of U/u_* plotted against z'/z_0. The values d and z_o in COSMO were estimated assuming a logarithmic variation of U/u_* at $2\,H$ and $3\,H$ under neutral stratification using $k = 0.4$. This gave $d = 1.25\,\mathrm{m}$ ($= 0.87\,H$) and $z_o = 0.09\,\mathrm{m}$ ($= 0.06\,H$). These values are similar to those obtained in wind-tunnel experiments (e.g. Cheng & Castro 2002), although they are merely rough estimates. The relationship between U/u_* and $z'u_*/\nu$ assures us that the flow within the inertial layer of COSMO is completely rough (not shown).

4. Results

4.1. *Spectral analysis*

We used spectral analysis to evaluate the eddy scales and their contribution to the total kinetic energy. The turbulent spectra and cospectra were calculated with a fast Fourier transform. The raw frequency f was converted to a wavenumber using Taylor's frozen hypothesis with local mean velocity U at each effective height z'. The spectra S_u, S_v, S_w, as well as Co_{uw} and wavenumber, were normalized by inner-layer variables so that $\overline{S_u} = S_u u_*^{-2}$, $\overline{S_v} = S_v u_*^{-2}$, $\overline{S_w} = S_w u_*^{-2}$, $\overline{Co_{uw}} = -Co_{uw} u_*^{-2}$ and $f' = fz'/U$. Spectra and cospectra corresponding to each non-dimensional frequency were ensemble averaged for every height.

Figures 7 and 8 show these results in pre-multiplied form (i.e. spectra multiplied by frequency) with log–log axes and log–linear axes, respectively. The values obtained by Kaimal *et al.* (1972), which are based on observations over a flat and rural surface, are also included in figures 7 and 8 as a relatively flat field. As shown in figure 7, all spectra at a frequency higher than 1.0 collapse to a $-2/3$ curve, which indicates that the spectra can be resolved to an inertial subrange.

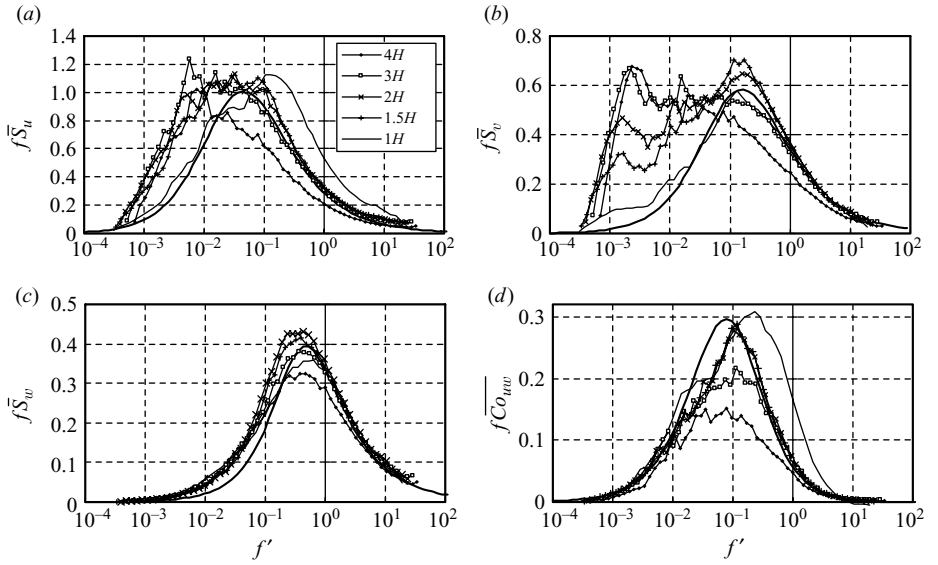

FIGURE 8. As figure 7, but plotted on log–linear axes.

In figure 8, we consider the spectral forms around the inertial layer, $z = 2H$. In the higher-frequency regions, all spectra and cospectra are close to the reference curves. In the lower-frequency region, however, $f\overline{S_u}$ and $f\overline{S_v}$ diverge from the reference curves. Figures 7 and 8 show that the forms of $f\overline{S_w}$ and $f\overline{Co_{uw}}$ agree relatively well with the reference curves over the complete wavenumber range.

The universality of all spectral curves in the high-frequency regions, irrespective of flat or rough surfaces, is strong evidence that the inner-layer scaling is valid because the characteristics of those eddies, which are the scale and magnitude of the fluctuation, are explained well by the inner-layer variables only. This supports Townsend's attached-eddy hypothesis with respect to the universal relationship between the turbulence and the wall, which implies that the eddy is wall-attached (Raupach *et al.* 1991).

On the other hand, the low-frequency fluctuations of the horizontal velocity did not follow the inner-layer scaling. These motions have their origins predominately in the outer-layer disturbance. In the atmospheric surface layer, the outer-layer disturbance is mainly attributed to the convective motion in the ABL, and their length scale is determined by the ABL depth (Kaimal *et al.* 1976; Panofsky *et al.* 1978) instead of the height above the ground. The ABL depth depends not only on the surface, but also on the synoptic conditions (Stull 1988). Therefore, the ensemble members of the data used in this analysis are obtained under various outer-layer conditions, and thus the scattering in the low-frequency part of spectra become large. However, the active eddies or fine-scale eddies still follow the inner-layer scaling. This implies that such a small eddy is irrelevant to the outer-layer scaling and is self-similar. Such a low-frequency fluctuation is interpreted as an inactive eddy (Bradshaw 1967*b*; Townsend 1976). Townsend (1976) indicated that inactive motion is imposed only on the horizontal velocity fluctuation, but not on the wall-normal velocity fluctuation or on the motion associated with the momentum transfer. Figure 8 shows that the largest difference from the rural reference is found in the low-frequency part of the streamwise spectra.

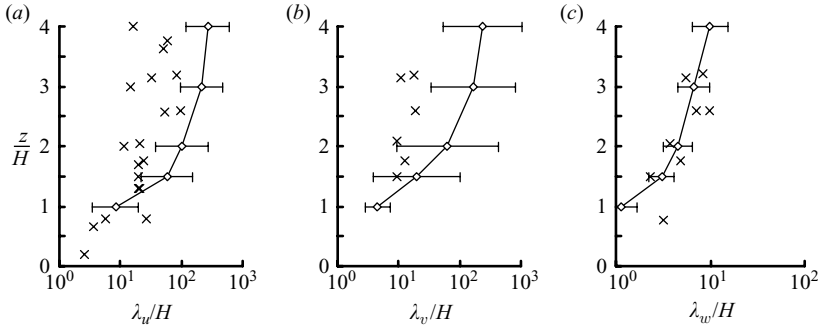

FIGURE 9. Vertical distributions of the peak wavelengths of spectra in COSMO normalized to mean obstacle heights: (*a*) streamwise velocity spectra, (*b*) spanwise velocity spectra, (*c*) wall-normal spectra. x, values obtained in urban experiments (reviewed by Roth 2000).

At the lowest level of measurement, the inner-scaled spectra and cospectra behave differently from those in the inertial layer. These spectral peaks are shifted to the higher frequencies, just as in the urban field experiment, although their energy content is somewhat different (e.g. Rotach 1995). The extra energy in the high-frequency region within the roughness sublayer is attributed to the wake production. The full expression of the TKE budget in the roughness sublayer, including the wake production term, is described by Raupach *et al.* (1986). The wake production is due to the local variation of the shear stress, which is associated with the wakes of individual roughness elements. Therefore, the scale of the wake production is related to the individual roughness elements. The difference in the spectral energy within the roughness sublayer can be attributed to the morphological differences in the building geometries.

Although there is still some debate about the turbulent structure within the roughness sublayer in cities, experimental studies (e.g. Roth 2000; Christen 2005) have suggested that the turbulent structure in the urban roughness sublayer is like that of a mixing layer with some modifications concerning the wake turbulence generated by sparse roughness elements. This is similar to a vegetation canopy (Raupach, Finnigan & Brunet 1996).

The spectra and cospectra at $4\,H$ are also different from the values at the other levels. The reason is that this level is above the inertial sublayer for COSMO owing to the limited length of fetch, and is within another internal boundary layer that develops from the upwind fetch or within the mixed layer, where the parameter u_* determined at $2\,H$ is no longer relevant to the turbulent fluctuations.

Next we compared the peak wavelength of the streamwise and vertical velocity spectra from COSMO and from full-scale cities to examine the similarity of an eddy scale that accounts for the major part of the TKE. The peak wavelength is obtained from the peak frequency of the spectra using λ_i, such as $\lambda_i = U/f_i'$ $(i = u, v, w)$.

Figure 9 shows the vertical variation of λ_u, λ_v and λ_w from COSMO and from cities. For practical reasons, λ_u, λ_v, λ_w and z are normalized by the mean roughness (building) heights for comparison with urban values given by Roth (2000). He used H for normalization to increase the variety of urban field measurements, having found that H roughly represents the length scale of roughness despite the variety of urban configurations. Our study builds on Roth's work and focuses on the geometrical similarity of the eddy scale for a variety of roughness scales.

Figure 9 shows that λ_u/H and λ_v/H in COSMO were one order larger than the values in cities, even allowing for their scattering. Such a difference would be

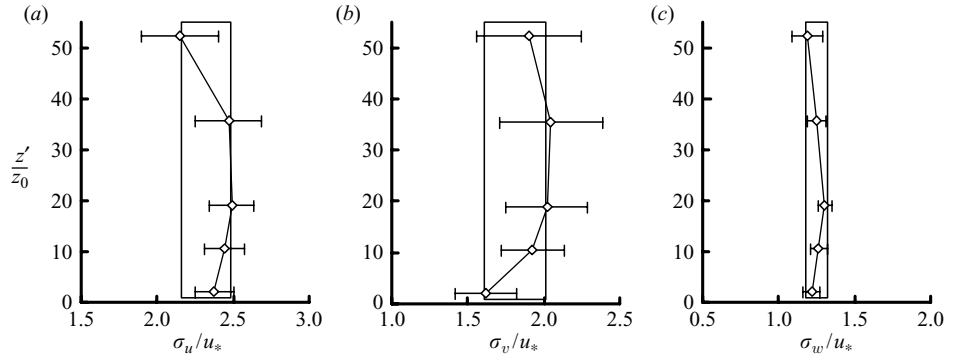

FIGURE 10. Vertical distributions of the non-dimensional velocity variance: (*a*) streamwise velocity, (*b*) spanwise velocity, (*c*) wall-normal velocity. The solid rectangular frame is the urban reference (Roth 2000).

introduced by the scaling variable, H, since the rate of the difference of λ_u/H (or λ_v/H) in COSMO and cities was the same as that of H. This implies that the values λ_u and λ_v are irrelevant to roughness, but relevant to the outer-layer variables (e.g. Kaimal *et al.* 1972).

The values of λ_w/H are about the same as those obtained in cities, as shown in figure 9(*c*). This means that the peak wavelength of the wall-normal velocity fluctuation is proportional to the roughness scale. Townsend (1976) explained the structure of near-wall turbulence in his attached-eddy hypothesis, saying that the turbulent motion in the turbulent boundary layer is the superposition of geometrically similar eddies. Our results partially support his hypothesis with respect to the scale of eddies over a fully rough surface in the atmosphere.

4.2. *Standard deviation of the velocity fluctuation*

The values of σ_u/u_*, σ_v/u_* and σ_w/u_* obtained from COSMO were analysed with inner-layer scaling. In accordance with MOS, these non-dimensional variables should be constants within the constant-stress layer under neutral stratification, independent of the scale and type of surface roughness.

Figure 10 shows σ_u/u_*, σ_v/u_* and σ_w/u_* plotted against the non-dimensional effective height z'/z_0. The solid line represents the average of the urban values in the inertial layer (Roth 2000). There is a peak value of both σ_u/u_*, σ_v/u_* and σ_w/u_* in the inertial layer, similar to the wind-tunnel experiments (Raupach *et al.* 1980; Cheng & Castro 2002), although the magnitudes in COSMO are larger than in the laboratory experiments. Their statistical scattering of σ_u/u_* and σ_v/u_*, expressed by the error bars, was also large. This indicates the failure of inner-layer scaling and the existence of some other relevant scaling for σ_u/u_* and σ_v/u_*. The scattering of σ_w/u_* is much smaller than that of the horizontal velocity components. The values σ_u, σ_v and σ_w are equal to the square root of the frequency integral of the corresponding spectra (figure 8). We showed that the turbulent spectra within the inertial layer are composed of high-frequency motions that follow the inner-layer scaling and low-frequency motions that can be attributed to the outer-layer disturbance. Since the u and v fluctuations come mostly from the outer-layer disturbance, as shown by the analysis of their spectral peaks, the statistical scattering in σ_u and σ_v with inner-layer scaling becomes larger. The major part of the w fluctuation follows the inner-layer scaling, and the scattering of σ_w/u_* is much smaller.

The values σ_u/u_* and σ_v/u_* in COSMO are larger than the urban average. The different outer-layer conditions is one possible explanation; however, it is not enough to account for the larger COSMO values because the scales of the outer-layer disturbance are comparable between COSMO and cities, as shown by the spectral peaks. This is further discussed in § 5.

The values at the lowest measurement level are smaller than those in the inertial layer. This result qualitatively follows the mixing-layer analogy and is similar to the vegetated roughness sublayer (Raupach *et al. 1996*, Finnigan 2000).

5. Discussion

In the previous section, we showed that the influence of the outer-layer disturbance was evident in the turbulent statistics with inner-layer scaling. In this section, we further quantify the relative importance of inner- and outer-layer disturbances in σ_u/u_*, σ_v/u_* and σ_w/u_* by decomposing the velocity fluctuations into the contributions from the inner- and outer-layer fluctuations based on the techniques of McNaughton & Laubach (1998) and on Townsend's (1976) original hypothesis about active and inactive eddies.

5.1. *Decomposing velocity fluctuations into inner- and outer-layer scale disturbances*

Townsend (1976) hypothesized that the turbulent boundary layer is the superposition of active and inactive eddies. An active eddy is the wall-related eddy and contributes to the momentum transfer. An inactive eddy originates in the outer-layer swirling motion, which is so large that the motion is two-dimensional in the near-wall region and it does not contribute to the vertical velocity fluctuations or vertical momentum transfer. Therefore, the active eddy scales with the inner-layer variables, and the inactive eddy scales with the outer-layer variables. There is no strong interaction between the active and inactive fluctuations if the Reynolds number is sufficiently high.

Based on the definition of active and inactive turbulence introduced by Townsend, the turbulent motions are decomposed into active and inactive contributions similar to the approach used in other studies (e.g. McNaughton & Laubach 1998; Zhao & Smits 2007). Since the equations about the streamwise and spanwise velocity fluctuations are entirely similar, only those for the streamwise velocity component are shown here.

$$u = u_{in} + u_{out}, \tag{7}$$

$$w = w_{in} + w_{out}, \tag{8}$$

where the primed quantities indicate the component fluctuating from the mean value, and the subscripts *in* and *out* denote the contribution from the active and inactive eddies, respectively. A practical way to decompose the natural values of u and w was proposed by McNaughton & Laubach (1998), although in this study we did not directly decompose the natural signals. Based on equations (7) and (8), we decompose the variances $\overline{uu}$ and $\overline{ww}$, and covariance $\overline{uw}$ into the contributions of the active and inactive eddies. The overbar denotes the ensemble average.

Following Townsend's hypothesis, the active turbulence only contributes to the momentum transfer, and inactive turbulence does not contribute to either the vertical motion or the momentum transfer. The active and inactive eddies have little interaction in high-Reynolds-number turbulent flow. Following these assumptions, the terms $u_{in}u_{out}$, $w_{in}w_{out}$, $u_{out}w_{out}$, $u_{in}w_{out}$, $u_{out}w_{in}$ and $w_{out}w_{out}$ are deemed to be

negligible. The ensemble average, the variances and covariance can then be written as

$$\overline{uu} = \overline{u_{in}u_{in}} + \overline{u_{out}u_{out}}, \tag{9}$$

$$\overline{ww} = \overline{w_{in}w_{in}}, \tag{10}$$

$$\overline{uw} = \overline{u_{in}w_{in}}. \tag{11}$$

The square of σ_u/u_* and σ_w/u_* are expressed by

$$\left(\frac{\sigma_u}{u_*}\right)^2 = \frac{\overline{uu}}{\overline{uw}} = \frac{\overline{u_{in}u_{in}} + \overline{u_{out}u_{out}}}{\overline{u_{in}w_{in}}} = \alpha_u + \frac{\overline{u_{out}u_{out}}}{\overline{u_{in}w_{in}}}, \tag{12}$$

$$\left(\frac{\sigma_w}{u_*}\right)^2 = \frac{\overline{ww}}{\overline{uw}} = \frac{\overline{w_{in}w_{in}}}{\overline{u_{in}w_{in}}} = \alpha_w. \tag{13}$$

The terms $\overline{u_{in}u_{in}}$ and $\overline{u_{in}w_{in}}$ ($\overline{w_{in}w_{in}}$ and $\overline{u_{in}w_{in}}$) have a linear relationship because the both follow the inner-layer scaling and their ratio is the constant α_u (α_w). The terms $\overline{u_{out}u_{out}}$ and $\overline{u_{in}w_{in}}$ are independent.

These equations indicate that the horizontal velocity fluctuation with inner-layer scaling is not constant owing to the propagation of the outer-layer disturbance into the inertial layer. Its effect appears in the second term of the right-hand side of equation (12) in the form of a ratio between the active and inactive disturbances. The relative contribution of the active and inactive eddies depends on the magnitude of the inactive eddy and also on the types of roughness because a difference in the surface geometry changes the magnitude of an active eddy even if the inactive eddy remains constant. The validity of these formulae is discussed along with the above two scenarios.

5.2. *Influence of the outer-layer disturbance*

We evaluated the impact of the outer-layer disturbance on the velocity fluctuations in the near-surface region. The evaluation was conducted using the data obtained from the COSMO experiment where the outer-layer disturbance changes owing to normal variations in the atmospheric conditions. The strength of the outer-layer disturbance is represented by the ABL depth z_i (Kaimal *et al.* 1976; Panofsky *et al.* 1978).

Unfortunately, we did not measure the value z_i directly during our experiment. Instead, we used the peak frequency of the horizontal velocity spectra $f'_{u_{peak}}$ obtained at $4H$, which represents the inverse of the ABL depth. This method was also used by Clarke *et al.* (1982) and Rotach (1993). As described in § 4.1, the inner- and outer-layer fluctuations contribute to the horizontal velocity fluctuation throughout the range of this experiment. The contribution of the inner-layer fluctuation is stronger closer to the surface. Therefore, the value $f'_{u_{peak}}$ indicates the outer-layer scale more clearly at higher elevations. The estimated length scale of the outer-layer fluctuation in COSMO is shown in figure 7(*a*); it is in the range of 100–600 m, which is consistent with the typical ABL winter depth in this region (e.g. Seino *et al.* 2003).

The values of σ_u/u_* and σ_w/u_* are plotted as functions of $f'_{u_{peak}}$ in figure 11, which shows that σ_u/u_* decreases as $f'_{u_{peak}}$ decreases. This supports equation (12). Figure 12 shows the friction velocity u_* plotted as a function of $f'_{u_{peak}}$. There is little correlation between u_* and $f'_{u_{peak}}$. Therefore we can attribute the main cause of the σ_u/u_* variations to the change of $\overline{u_{out}u_{out}}$ as a function of $f'_{u_{peak}}$. These trends were observed in the rural experiments (Kaimal *et al.* 1976; Panofsky *et al.* 1978) and also in the urban experiments based on equation (6) (Clarke *et al.* 1982; Rotach 1993). Meanwhile, the values σ_w/u_* are largely independent of $f'_{u_{peak}}$. This is expected because the outer-layer

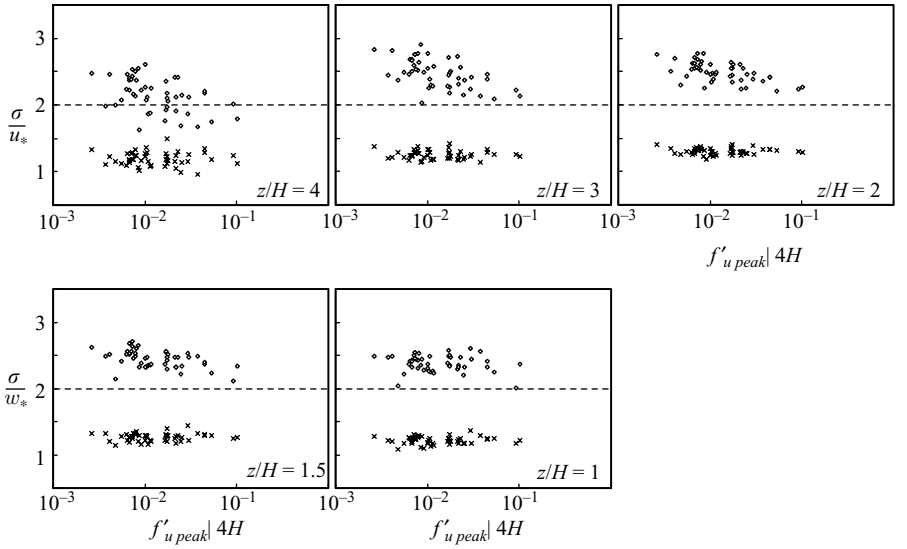

FIGURE 11. Non-dimensional standard deviations of velocity fluctuations plotted against the peak frequency of the spectra obtained at $4\,H$. $\diamond$, σ_ω/u_*; x, σ_ω/u_*.

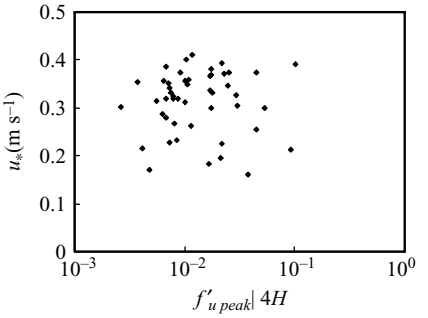

FIGURE 12. Friction velocities plotted against the peak frequency of the spectra obtained at $4\,H$.

disturbance is hardly a factor in the vertical velocity component, and such a large-scale vertical motion is damped by the presence of the surface and diverges in the near-surface region.

Although the values σ_u/u_* varied according to the ABL depth, they were never less than 2.0 in the inertial layer. According to (12), the lowest values are obtained when there is no prominent outer-layer disturbance, which is induced by buoyant forcing or outer-layer mechanical forcing independent of the surface friction in COSMO. Such a canonical condition is only available in the laboratory or in numerical experiments where all turbulence can be attributed to surface friction. The values σ_u/u_* are usually about 2.0 in a wind tunnel (e.g. Raupach *et al.* 1991) and in large-eddy simulations (e.g. Kanda *et al.* 2004). Therefore, the universal constant α is expected to be about 4.0 for streamwise velocity fluctuations. This is also supported by Panofsky *et al.* (1978) in experiments over flat fields and water.

Further examination of figure 11 reveals that the slope of σ_u/u_* as a function of $f'_{u_{peak}}$ becomes flatter for decreased measurement heights. The reason for this change of slope is probably that the contribution of the outer-layer disturbance is weakened

by the damping at the rigid wall, or by the relatively stronger inner-layer disturbance close to the roughness.

5.3. *Relative scale of the inner and outer layers*

The influence of the outer-layer disturbance on the values of σ_u/u_* and σ_w/u_* was confirmed for the COSMO data in the previous section. In this section, we use a common analytical framework to compare the values of σ_u/u_*, σ_w/u_* and also σ_v/u_* obtained from various other experiments. According to (12) and (13), the value of σ_u/u_* depends on the ratio of inner- and outer-layer variables, but that of σ_w/u_* does not. As a simple measurement, the relative scale of the inner and outer layers (z_o/z_i) is used as a common index for comparison. The inner- and outer-layer scales are represented by z_o and z_i, respectively.

We compared the values σ_u/u_*, σ_v/u_* and σ_w/u_* from various data sources including COSMO, urban experiments (Roth 2000), rural experiments (Högström 1990) and wind-tunnel experiments (Raupach *et al.* 1991). The roughness length z_o in these data ranges varied widely: 1.0–10 m for urban experiments, 0.1 m for COSMO, 0.01 m for rural experiments and 0.0001 m for a rough surface in a wind tunnel. The boundary-layer heights, z_i, in COSMO were estimated from the spectral peak of the horizontal velocity fluctuations obtained at $4H$. Using $z_i = 1.5\lambda_u$ (Kaimal *et al.* 1976) gave a range of several 100 m, which is consistent with the observed values near this region in winter (Seino *et al.* 2003). The values of z_i for the other atmospheric fields were assumed to be a constant value of 1000 m. This is a very rough assumption, but it is not critical to the value of z_o/z_i because while z_i is almost the same order, z_o is a few orders different in our comparison.

The values of σ_u/u_*, σ_v/u_* and σ_w/u_* are plotted against z_o/z_i in figure 13. The values of σ_u/u_* and also σ_v/u_* decrease slightly with increasing z_o/z_i for COSMO and field observations, as expected from (12). The plots of σ_v/u_* are rather scattered in comparison with those of σ_u/u_*, whereas the values from wind-tunnel experiments go to a lower limit of about 2.0 for σ_u/u_* and 1.3 for σ_v/u_*. The value of σ_w/u_* does not vary much with z_o/z_i; this reflects the fact that the outer-layer disturbance is insensitive to the vertical velocity fluctuation, as shown in figures 10 and 11. Although we used an empirical value for the ABL height (500 m) for 'rural' and 'urban' in figure 13, the result does not change the current discussion.

Some experimental studies of urban regions have disagreed as to whether σ_u/u_*, σ_v/u_* and σ_w/u_* depend on z_o (Clarke *et al.* 1982; Yersel & Goble 1986; Roth 2000). According to our work, z_o/z_i should be used for σ_u/u_* and σ_v/u_* instead of z_o. Such contrasting observations are possible owing to the narrow range of z_o and the lack of reliable estimations of z_i in real cities. The data for real cities actually exhibit larger scattering than shown in figure 13. However, over the full range of z_o/z_i from flat surfaces, COSMO and real cities, the dependency of σ_u/u_* and σ_v/u_* on z_o/z_i becomes clear. We did not observe any dependence of σ_w/u_* on z_o/z_i.

It is significant that the value of σ_u/u_* and σ_v/u_* from wind-tunnel experiments is always close to the lower limit of the atmospheric values. This is probably because no prominent outer-layer disturbance is generated in wind-tunnel experiments, even for very small values of z_o/z_i. On the other hand, the value of σ_u/u_* from Yersel & Goble (1986) is significantly larger than that from the urban experiments reported by Roth (2000). His measurement site was in rolling terrain. Raupach *et al.* (1991) also reviewed the value above rolling terrain, which is comparably large and greater than 3.0. The topographical variation probably mechanically induced an additional ABL

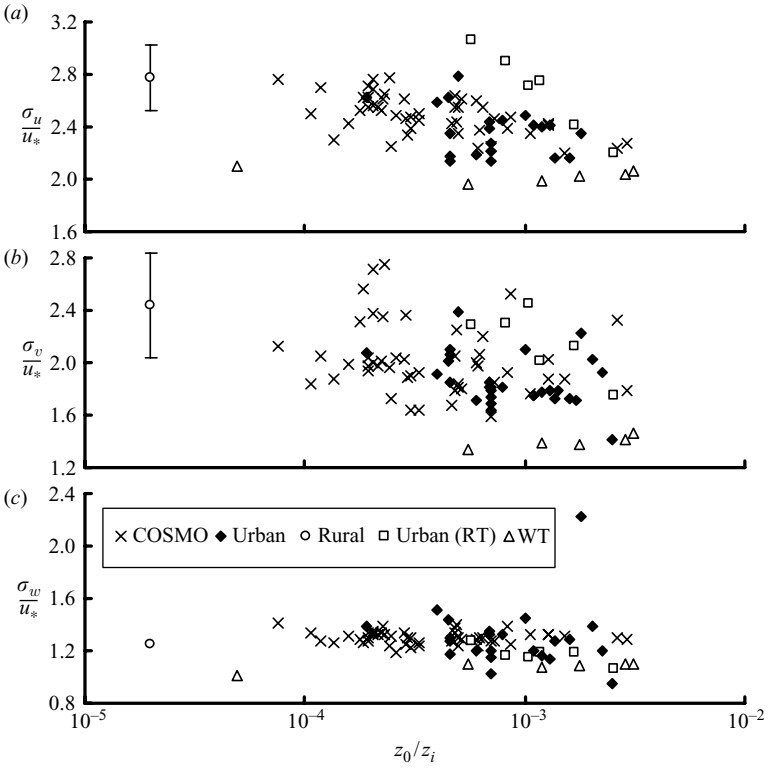

FIGURE 13. Non-dimensional velocity variances plotted against the non-dimensional aerodynamic roughness length: (*a*) streamwise velocity, (*b*) spanwise velocity, (*c*) wall-normal velocity. The values are from the following studies: ×, COSMO; ◇, Urban (Roth 2000; Clarke *et al.* 1982); ○, Rural (Högström 1990); □, Urban (RT) (urban in rolling terrain; Yersel & Goble 1986); △, WT (wind tunnel; Raupach *et al.* 1991).

scale of turbulent mixing (Stull 1988), resulting in the enhancement of the outer-layer disturbance.

6. Conclusions

The inner-layer scale similarity worked well for the wall normal fluctuation and the Reynolds stress, independent of the surface roughness or the outer-layer conditions under near-neutral stratification and in atmospheric flow. This implies that there are always wall-related eddies that are similar, as predicted by the attached-eddy model, and they are less connected with the outer-layer disturbance.

The inner-layer scale similarity failed only for horizontal velocity fluctuations owing to the influence of the outer-layer disturbance. We evaluated the relative contribution of the outer-layer disturbance to the inner-scaled horizontal velocity fluctuations. The ratio between the outer- and inner-layer eddy scales is important for estimating the inner-scaled horizontal velocity fluctuation.

The form of the streamwise velocity spectra in COSMO was similar to that found in high-Reynolds-number turbulent flows in pipes (e.g. Kim & Adrian 1999; Guala, Hommema & Adrian 2006) with respect to the existence of the f^{-1} region, which is associated with the occurrence of very large-scale motion (VLSM). However, it is still not clear how similar the flows in pipes and ASL actually are, especially for

the structural characteristics of low-frequency motions. In the case of the ASL, such low-frequency motion is attributed to the convective mixing in the ABL, and it is inactive. It is not a trivial matter to study ABL-like convection in pipe flow.

Additional experiments in COSMO revealed that relatively low-speed regions form large-scale streaks, which are similar to the VLSM proposed by Kim & Adrian (1999). They are very large; about 10 m ($100z_o$) in the spanwise direction and more than 100 m ($1000z_o$) in the streamwise direction. This large structure accounted for a major part of the momentum transport. This will be discussed in greater detail in the next report on the COSMO experiment, which will focus on the spatially coherent structures of the turbulent motion.

Finally, as shown by Kunkel & Marusik (2006), the atmospheric flow still depends on the Reynolds number, even though the number is very high. We did not address this phenomenon in this paper since the effect of the prominent outer-layer disturbance in the atmosphere, which is mostly independent of the Reynolds number within the inertial layer, has a larger effect on the horizontal velocity fluctuation than the Reynolds number does.

This research was financially supported by the Core Research for Evolution Science and Technology program of the Japanese Science and Technology Cooperation and Grant-in-Aid for JSPS Fellows. We wish to thank Dr Hirofumi Sugawara for his useful comments concerning the mixed layer height.

REFERENCES

Akinlade, O. G., Bergstrom, D. J., Tachie, M. F. & Castillo, L. 2004 Outer flow scaling of smooth and rough wall turbulent boundary layer. *Exps. Fluids* **37**, 604–612.

Bradshaw, P. 1967*a* The turbulence structure of equilibrium boundary layers. *J. Fluid Mech.* **29**, 625–645.

Bradshaw, P. 1967*b* Inactive motions and pressure fluctuations in turbulent boundary layers. *J. Fluid Mech.* **30**, 241–258.

Cheng, H. & Castro, I. P. 2002 Near wall flow over urban-like roughness. *Boundary-Layer Met.* **104**, 229–259.

Christen, A. 2005 Atmospheric turbulence and surface energy exchange in urban environments. PhD thesis, *University of Basel*.

Clarke, J. F., Ching, J. K. S. & Godowitch, J. M. 1982 An experimental study of turbulence in an urban environment. *Tech. Rep. USEPA*, Research Triangle Park, NC. NMS PB 226085.

Coceal, O., Thomas, T. G., Castro, I. P. & Belcher, S. E. 2006 Mean flow and turbulence statistics over groups of urban-like cubical obstacles. *Boundary-Layer Met.* **121**, 491–519.

Cui, J., Patel, V. V. & Lin, C. L. 2003 Large-eddy simulation of turbulent flow in a channel with rib roughness. *Intl J. Heat Fluid Flow* **24**, 372–388.

Finnigan, J. 2000 Turbulence in plant canopies. *Annu. Rev. Fluid Mech.* **32**, 519–571.

Guala, M., Hommema, S. F. & Adrian, R. J. 2006 Large-scale and very-large-scale motions in turbulent pipe flow. *J. Fluid Mech.* **554**, 521–541.

Hanna, S. R., Tehranian, S., Carissimo, B., MacDonald, R. W. & Lohner, R. 2002 Comparisons of model simulations with observations of mean flow and turbulence within simple obstacle arrays. *Atmos. Environ.* **36**, 5067–5079.

Högström, U. 1990 Analysis of turbulence structure in the surface layer with a modified similarity formulation for near neutral conditions. *J. Atmos. Sci.* **47**, 1949–1972.

Högström, U., Bergström, H. & Alexandersson, H. 1982 Turbulence characteristics in a near neutrally stratified urban atmosphere. *Boundary-Layer Met.* **23**, 449–472.

Jimenez, J. 2004 Turbulent flows over rough walls. *Annu. Rev. Fluid Mech.* **36**, 173–196.

Kaimal, J. C. & Finnigan, J. J. 1994 *Atmospheric Boundary Layer Flows.* Oxford University Press.

Kaimal, J. C., Wyngaard, J. C., Izumi, Y. & Cote, O. R. 1972 Spectral characteristics of surface layer turbulence. *Q. J. R. Met. Soc.* **98**, 563–589.

Kaimal, J. C., Wyngaard, J. C., Haugen, D. A., Cote, O. R. & Izumi, Y. 1976 Turbulent structure in the convective boundary layer. *J. Atmos. Sci.* **33**, 2152–2169.

Kanda, M. 2006 Large eddy simulations on the effects of surface geometry of building arrays on turbulent organized structures. *Boundary-Layer Met.* **118**, 151–168.

Kanda, M., Moriwaki, R. & Kasamatsu, F. 2004 Large eddy simulation of turbulent organized structure within and above explicitly resolved cubic arrays. *Boundary-Layer Met.* **112**, 343–368.

Kim, K. C. & Adrian, R. J. 1999 Very large-scale motion in the outer layer. *Phys. Fluids* **11**, 417–422.

Krogstad, P. A., Andersson, H. I., Bakken, O. M. & Ashrafian, A. 2005 An experimental and numerical study of channel flow with rough walls. *J. Fluid Mech.* **530**, 327–352.

Kunkel, G. J. & Marusic, I. 2006 Study of the near-wall-turbulent region of the high-Reynolds-number boundary layer using an atmospheric flow. *J. Fluid Mech.* **548**, 375–402.

McNaughton, K. G. & Raubach, J. 1998 Unsteadiness as a cause of non-equality of eddy diffusivities for heat and vapour at the base of an advective inversion. *Boundary-Layer Met.* **88**, 479–504.

Miyake, Y., Tsujimoto, K. & Nakaji, M. 2001 Direct numerical simulation of rough-wall heat transfer in a turbulent channel flow. *Intl J. Heat Fluid Flow* **22**, 237–244.

Nagano, Y., Hattori, H. & Houra, T. 2004 DNS of velocity and thermal fields in turbulent channel flow with transverse-rib roughness. *Intl J. Heat Fluid Flow* **25**, 393–403.

Panofsky, H. A. & Dutton, J. A. 1984 *Atmospheric Turbulence.* John Wiley.

Panofsky, H. A., Tennekes, H., Lenschow, D. H. & Wyngaard, J. C. 1978 The characteristics of turbulent velocity components in the surface layer under the unstable conditions. *Boundary-Layer Met.* **11**, 355–361.

Perry, A. E. & Abell, C. J. 1977 Asymptotic similarity of turbulence structures in smooth- and rough-walled pipes. *J. Fluid Mech.* **79**, 785–799.

Raupach, M. R., Thom, A. S. & Edwards, I. 1980 A wind tunnel study of turbulent flow close to regularly arrayed rough surfaces. *Boundary-Layer Met.* **18**, 373–397.

Raupach, M. R.,Coppin, P. A. & Legg, B. J. 1986 Experiments on scalar dispersion within a model plant canopy. Part I: The turbulence structure. *Boundary-Layer Met.* **35**, 21–52.

Raupach, M. R., Antonia, R. A. & Rajagopalan, S. 1991 Rough-wall turbulent boundary layers. *Appl. Mech. Rev.* **44**, 1–25.

Raupach, M. R., Finnigan, J. J. & Brunet, Y. 1996 Coherent eddies and turbulence in vegetation canopies: the mixing-layer analogy. *Boundary-Layer Met.* **78**, 351–382.

Rotach, M. W. 1993 Turbulence close to a rough urban surface. Part II: Variances and gradients. *Boundary-Layer Met.* **66**, 75–92.

Rotach, M. W. 1995 Profiles of turbulence statistics and above an urban street canyon. *Atmos. Environ.* **29**, 1473–1486.

Rotach, M. W. 1999 On the influence of the urban roughness sublayer on turbulence and dispersion – spectral characteristics. *Atmos. Environ.* **33**, 4001–4008.

Roth, M. & Oke, T. R. 1993 Turbulent transfer relationships over an urban surface. I: Spectral characteristics. *Q. J. R. Met. Soc.* **119**, 1071–1104.

Roth, M. 1993 Turbulent transfer relationships over an urban surface. II. Integral statistics. *Q. J. R. Met. Soc.* **119**, 1105–1120.

Roth, M. 2000 Review of atmospheric turbulence over cities. *Q. J. R. Met. Soc.* **126**, 941–990.

Seino, N., Yoshikado, H., Kobayashi, F., Sato, J. *et al.* 2003 Vertical structure of local fronts observed in Kanto, Japan. *J. Met. Soc. Japan* **81**, 367–391.

Stull, R. B. 1988 *An Introduction to Boundary Layer Meteorology.* Kluwer.

Thom, A. S. 1971 Momentum absorption by vegetation. *Q. J. R. Met. Soc.* **97**, 414–428.

Townsend, A. A. 1961 Equilibrium layers and wall turbulence. *J. Fluid Mech.* **11**, 97–120.

Townsend, A. A. 1976 *The Structure of Turbulent Shear Flow.* Cambridge University Press.

Willis, D. E. & Deardorff, J. W. 1976 On the use of Taylor's translation hypothesis for diffusion in the mixed layer. *Q. J. R. Met. Soc.* **102**, 817–822.

Yersel, M. & Goble, R. 1986 Roughness effects on urban turbulence parameters. *Boundary-Layer Met.* **37**, 271–284.

Zhao, R. & Smits, A. J. 2007 Scaling of the wall-normal turbulence component in high-Reynolds-number pipe flow. *J. Fluid Mech.* **576**, 457–473.